

## Comparison of the Performances of DCFC Fuelled with the Product of Methane RF Plasma Reforming and Carbon Black

M. Dudek<sup>1,\*</sup>, P. Tomczyk<sup>1</sup>, K.L. Juda<sup>2</sup>, R. Tomov<sup>2</sup>, B.A. Glowacki<sup>2,3</sup>, S. Batty<sup>4</sup>, P. Risby<sup>4</sup>, R. Socha<sup>5</sup>

<sup>1</sup> AGH - University of Science and Technology, Faculty of Fuels and Energy, Av. Mickiewicza 30, 30-059 Cracow, Poland,

<sup>2</sup> Department of Materials Science and Metallurgy, University of Cambridge, Pembroke Street, Cambridge CB2, 3QZ, United Kingdom

<sup>3</sup> Institute of Power Engineering, ul Augustówka 6, 02-981 Warsaw, Poland

<sup>4</sup> GasPlas GaAS, Parkveien 57, 0256 Oslo, Norway

<sup>5</sup> Jerzy Haber Institute of Catalysis and Surface Chemistry, Polish Academy of Science, Niezapominajek 8, 30-239 Cracow, Poland

\*E-mail: [potoczek@agh.edu.pl](mailto:potoczek@agh.edu.pl)

*Received:* 7 June 2012 / *Accepted:* 11 July 2012 / *Published:* 1 August 2012

---

Development of direct carbon fuel cells opens new options for utilization of various carbonaceous fuels to produce electricity. Moreover, even some waste materials and by-products from industrial processes appear to be suitable for conversion in DCFC. An attractive opportunity is the use of carbon based by-products of methane plasma dissociation as a fuel. In this work comprehensive studies of two types of carbon fuels were performed, namely carbon powder (carbon A) produced by methane plasma dissociation and commercially available carbon black powder (carbon B). Before the electrochemical testing, both carbon fuels were characterized by X-ray, Raman, XPS/ESCA spectroscopy, thermal analysis (DTA, TG), electrical conductivity and other methods. Carbon A possessed larger particle surface area and lower ohmic resistance than carbon B, its purity was comparably high and ash content was low. Four different types of DCFCs were used during testing: all of them used solid electrolyte (8YSZ) and varied only anodic part of the cells. All the tests showed high degree of feasibility of the waste product of methane plasma splitting (carbon A) as a fuel for DCFC, very similar to the traditionally used as a reference carbon B.

---

**Keywords:** carbon, direct carbon fuel cell, methane plasma splitting, carbon black

### 1. INTRODUCTION

The decline of the petrochemical oil reserves and the evidence of global warming along with the steadily increasing world demand for energy have initiated intensive search for new more efficient

electricity generation techniques and carbon sequestration technologies. Fuel cells (FC) are one of the most promising energy conversion technologies characterised by their high efficiency compared to internal combustion engine [1, 2]. Hydrogen is commonly used as fuel in variety of FC's working in different temperature ranges and built on different materials bases. At present, steam reforming of methane is the most widely used and economical method for production of hydrogen. Unfortunately the process is accompanied by emission of greenhouse gases (mainly CO<sub>2</sub> and CO) and requires centralised production and distribution infrastructure [3-5]. The CO<sub>x</sub>-free hydrogen production methods, like water electrolysis and ammonia decomposition, are characterised by higher energy costs and currently contribute only a fraction to the worldwide hydrogen production capacity [6-8]. Non-thermal plasma decomposition of methane offers an environmentally friendly and energy efficient production of pure hydrogen and solid carbon particles [9,10]. The carbon is usually considered as a by-product, although some potentially useful forms of carbon, including graphite and variety of nanoforms, can be produced in this process [11].

Direct carbon fuel cells (DCFC) have a long and uneven history [12,13]. DCFC research has undergone recent renaissance attracting a renewed interest and encompassing variety of fuel cell configurations and approaches. All these efforts are aimed at practical and economically feasible conversion of different carbonaceous solids (coal, biomass, coke, municipal solid waste) directly to electric power [14,15].

The interest in DCFC is driven by the prospect of direct utilization of the abundant solid carbon reserves and the high efficiency of power generation reaching practically up to 80%, compared to traditional coal-fired power plants efficiency (~40-50%). Additional benefits include the established carbon delivery infrastructure and the easy storage. Pure carbon oxidation product (CO<sub>2</sub>) of the DCFC is suitable for direct sequestration without expensive gas separation and energy-intensive purification processes [16]. A new and promising direction for DCFC technology is the utilization of the carbon by-product from plasma reforming of methane.

Various types of DCFC have been recently investigated. One of the most popular classifications is based on the type of electrolyte used in the cell - alkaline environment, molten carbonate and solid oxide electrolytes. The latter system, DC-SOFC, is considered promising due to uncomplicated maintenance, although the power density reported so far remain relatively low [17,18]. This is a result of a limited reaction zone restricted to the direct contacts between the carbon particles and the solid oxide electrolyte. Further development and commercialisation of DC-SOFC requires significant improvements in the efficiency of direct conversion of carbon fuels into electricity and the fuel utilization [19].

Implementation of composite carbon-based fuels providing extended reaction zone for carbon electrooxidation to the whole volume of the DC-SOFC is critical for the improvement of the DCFC performance. Currently, the hybrid carbon fuel cell (HDCFC) concept, which combines the technological achievements of both, molten carbonate fuel cell (MCFC) and solid oxide fuel cell (SOFC), is one of the most frequently proposed option for performance improvement of DC-SOFC. In HDCFC system, the carbon particles are mixed in Li<sub>2</sub>CO<sub>3</sub>-K<sub>2</sub>CO<sub>3</sub> or Li<sub>2</sub>CO<sub>3</sub>-Na<sub>2</sub>CO<sub>3</sub> molten eutectic and as-prepared composite fuel is introduced into the anode chamber of SOFC cell. During the SOFC operation at temperatures 700-900°C, carbon particles become dispersed in the molten carbonate

eutectic, resulting in an increase of the reaction zone where the carbonate ions are directly involved in the electrochemical oxidation of carbon fuel [20,21].

The aim of this paper is to examine the effect of the properties of different carbon fuels on the performance of DC-SOFC. Special emphasis is put on the utilization of carbon by-product of methane plasma dissociation. The ultimate goal is to verify the feasibility of RF plasma methane conversion products as fuels for DCFC.

## 2. EXPERIMENTAL

In order to provide a comparative interpretation of the performance data, two different types of carbon fuels were investigated in parallel:

- Carbon, product obtained from RF plasma methane splitting, named hereafter as carbon (A)
- Commercial carbon black powder (N-220), named hereafter as carbon (B)

### 2.1. Production of carbon by plasma splitting of methane; Carbon A

The natural gas plasma reforming was conducted in a standard RF plasma reactor equipped with 2.5GHz magnetron. The flow rate of natural gas - N<sub>2</sub> mixture (20:1 volume ratio) was supplied from compressed gas cylinders under normal pressure. The flow rate of both gases was adjusted using mass flow controllers. The microwave non-equilibrium plasma was sustained in the section of the quartz tube passing through the waveguide where a maximum E-field was located. Natural gas flow was adjusted at the rate of 40 l/min (stp, +/- 10%) entering the plasma produced by a 5 KW emf (+/- 5%) microwave source. The mixture of CH<sub>4</sub> and N<sub>2</sub> was injected into one end of the quartz tube by means of tangentially directed orthogonally oriented narrow slits so as to induce a strong vortex motion in the discharge zone. A rotating column of gas streams was created aiding the gas mixing and plasma stabilization, and helping to avoid the quartz tube burning. The natural gas was thus dissociated into carbon and hydrogen ions and radicals.

### 2.2. Commercial carbon black powder (N-220); carbon (B)

The carbon black is frequently used as a fuel in the DCFC technology research [22, 23]. We utilized the same type (N-220) of carbon powder in our previous studies [24] as a reference material for our laboratory DC-SOFC. Carbon (B) is a commercial product supplied by Komimpex, Poland.

### 2.3 Analytical methods of carbon evaluations

The phase composition of the carbon powders (A) and (B) were evaluated by X-ray diffraction analysis referring to the ICDD database. XRD measurements were done using the Panalytical X'Pert Pro system with monochromatic CuK<sub>α</sub> radiation. Specific surface area was determined by multipoint

nitrogen adsorption at  $-196^{\circ}\text{C}$  (Quantachrome Pore Master). A transmission electron microscopy (AEM Philips) coupled with an EDS system was used to characterise the morphology and chemical composition of the carbon particles. The thermal effects occurring during heating of the solid carbon fuel in a temperature range of  $25\text{-}1000^{\circ}\text{C}$  in helium gas flow were measured by DTA and TG methods (SDT 2960 TA Instruments). The samples (ca. 50 mg) were ramped-up at  $10\text{ K}\cdot\text{min}^{-1}$  rate in an alumina crucible.

Chemical surface analyses of the carbon particles were performed by a XPS/ESCA method with a hemispherical analyser (SES R 4000, Gammadata Scienta). The spectra were processed using Casa XPS 2.3.12 software while the background was approximated by a Shirley profile. The spectra deconvolution into a minimum number of components was done by an application of Voigt-type line shapes. Raman spectra of carbon particles were collected using a FTS 6000 Bio-Rad Spectrometer with Raman section (Nd: YAG Spectra Physics T10, 1064 nm laser). The spectra were collected after 10,000 scans at  $4\text{ cm}^{-1}$  resolution. The electrical resistivity measurements of carbon pellets were performed by a four probe a.c. method in a temperature range of  $30\text{-}800^{\circ}\text{C}$  in argon flow.

The direct electrochemical oxidation of carbon was studied using four types of electrochemical cell, varying only in the anodic part of the cell:

- a) C|8YSZ|LSM-GDC|LSM|O<sub>2</sub>
- b) C+(Li<sub>2</sub>CO<sub>3</sub>-Na<sub>2</sub>CO<sub>3</sub>) eut. |8YSZ|LSM-GDC|LSM|O<sub>2</sub>
- c) C|Ni-YSZ|8YSZ|LSM-GDC|LSM|O<sub>2</sub>
- d) C+(Li<sub>2</sub>CO<sub>3</sub>-Na<sub>2</sub>CO<sub>3</sub>) eut. |Ni-YSZ|8YSZ|LSM-GDC|LSM|O<sub>2</sub>

where:

- 8YSZ was 150  $\mu\text{m}$  thick electrolyte consisting of 8 mol % Y<sub>2</sub>O<sub>3</sub> in ZrO<sub>2</sub>, LSM was La<sub>0.8</sub>Sr<sub>0.2</sub>MnO<sub>3</sub> cathode material,
- LSM-GDC was composite cathode material made of LSM+10 mol % Gd<sub>2</sub>O<sub>3</sub> in CeO<sub>2</sub> (GDC),
- C+(Li<sub>2</sub>CO<sub>3</sub>-Na<sub>2</sub>CO<sub>3</sub>) was mixture of 1 g of carbon particles and 3 g of eutectic mixture of lithium and sodium carbonate.

The schematic of the four types of DC-SOFC, used in the experiments, are shown in Fig.1 a-d.

The cross – section view of the experimental set-up with a DC-SOFC placed inside is shown in Fig.2.

The cell consisted of two chambers separated by a button solid oxide fuel cells (1) (20 mm in diameter and ca.0.2 mm thick), which was fixed to Al<sub>2</sub>O<sub>3</sub> tubes (2) on each side. The cathode (3) was supplied with atmospheric air. The anode current collector (6) was a gold mesh welded to a gold wire (5) and covered with carbon fuel (4). The cell was located inside an electric furnace (7). During the experiment, argon was continuously supplied to the anodic chamber as a shield gas. The geometric area of the active electrolyte surface was estimated to be  $1.36\text{ cm}^2$ .

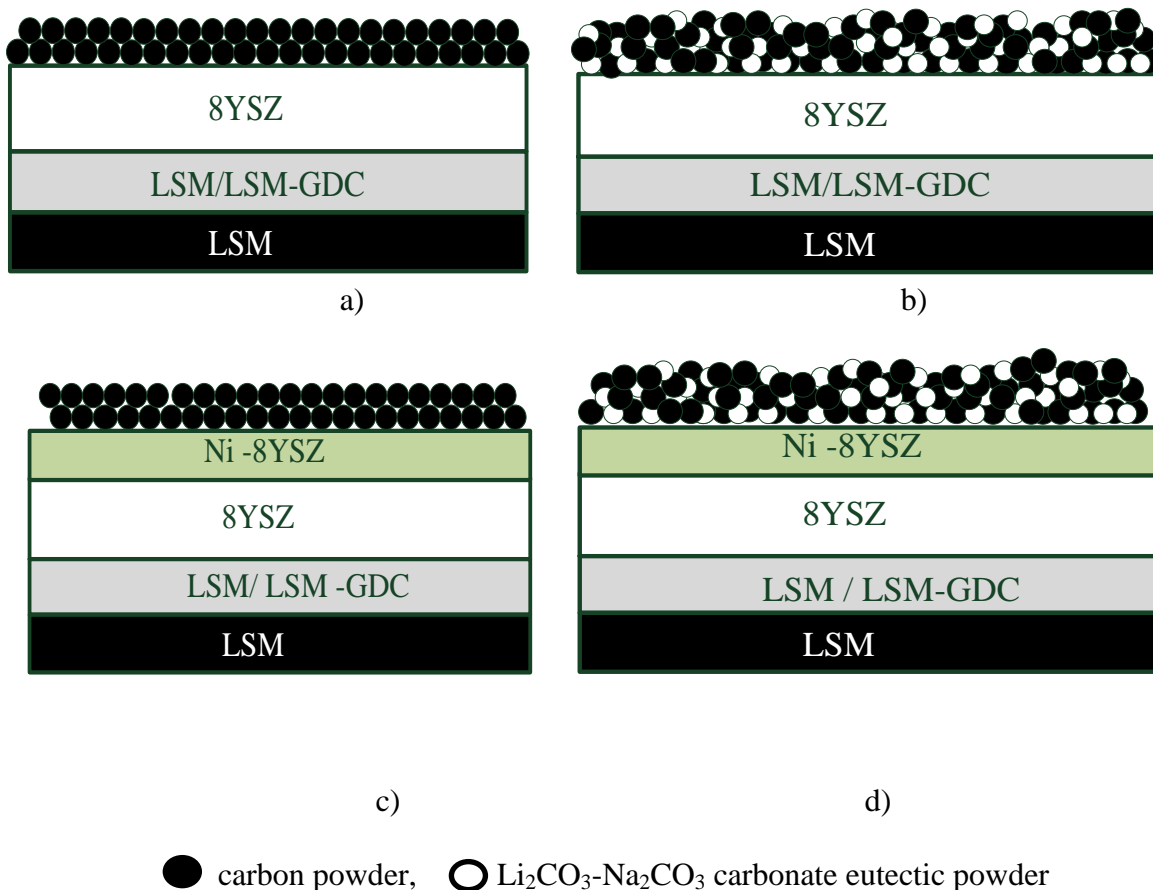


**Figure 1.** a-d Schematics of the four types of DC-SOFC: (a) C|8YSZ|LSM-GDC|LSM |O<sub>2</sub>; (b) C+(Li<sub>2</sub>CO<sub>3</sub>-Na<sub>2</sub>CO<sub>3</sub>) eut. |8YSZ|LSM-GDC|LSM|O<sub>2</sub>; (c) C|Ni-YSZ|8YSZ|LSM-GDC|LSM|O<sub>2</sub>; (d) C+(Li<sub>2</sub>CO<sub>3</sub>-Na<sub>2</sub>CO<sub>3</sub>) eut. |Ni-YSZ|8YSZ|LSM-GDC|LSM|O<sub>2</sub>

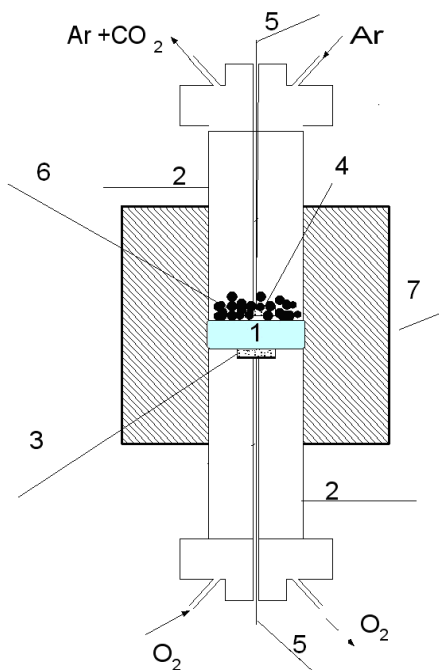


**Figure 2.** The side view of the DC-SOFC experimental setup

Electrochemical measurements were performed in a temperature range of 500-850 °C using a potentiostat PGSTAT 300N equipped with a GPES (CV) and FRA (EIS) modules. The impedance spectroscopy measurements were performed in the frequency range from 0.001 Hz to 1 MHz using 10 mV sinusoidal voltage amplitude. For analysis of the impedance data, a program provided by the vendor (Metrohm, Autolab B.V), based on a complex non-linear regression least-squares (CNRLS) fit was used.

### 3. RESULTS

The X-ray diffraction patterns, recorded for carbon powder (A) and carbon powder (B), are presented in Fig. 3 The XRD spectra were normalized towards the peak at  $2\theta = 20-26$  deg.

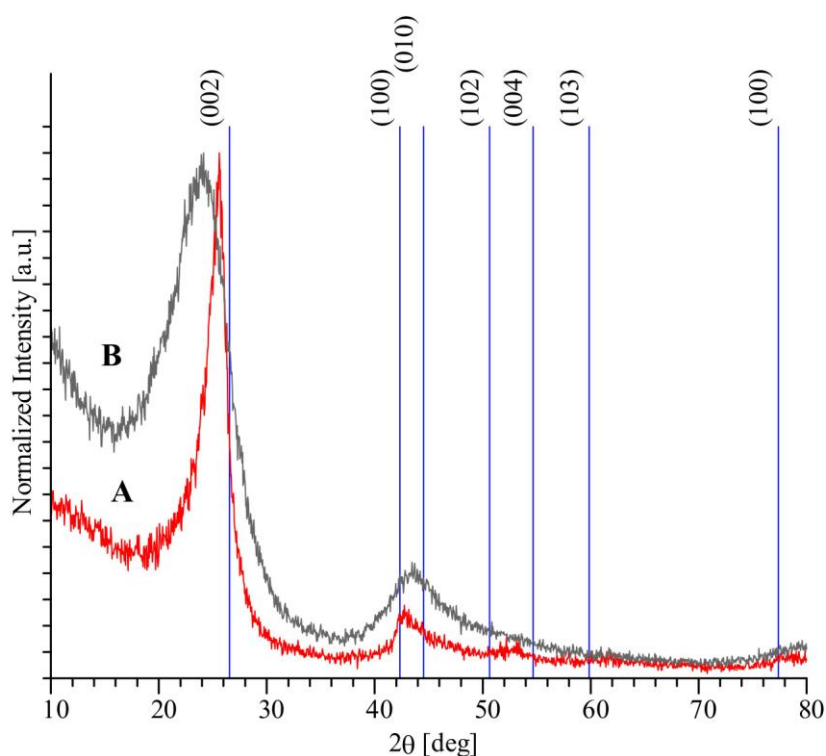
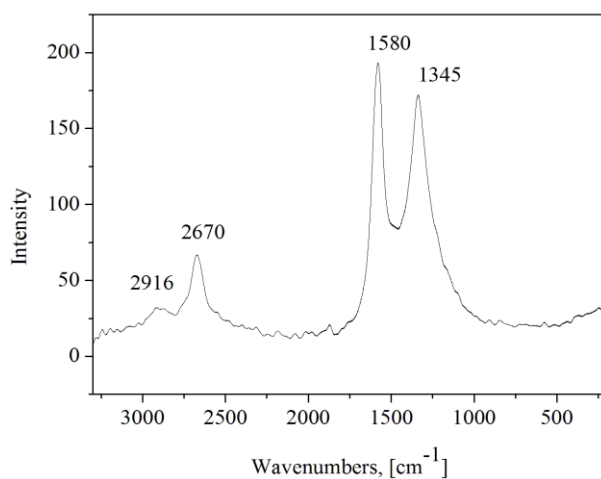


**Figure 3.** The X-ray diffraction pattern recorded for carbon (A) and (B) powders.

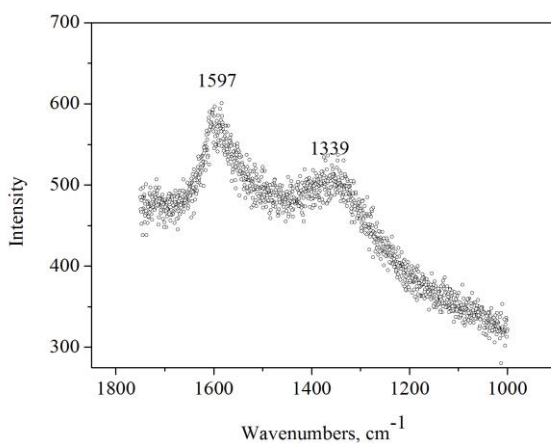
The vertical lines mark the position of the peaks corresponding to tabulated graphite diffraction patterns. Such patterns are rather typical for a disordered carbon phase [25]. The XRD patterns of the both carbons (A) and (B) reflect also what is likely a short range graphite or turbostratic structure of the sample [26,27].

Raman spectroscopy was applied as a method complementary to XRD diffraction analysis, further clarifying the structural properties of the carbon materials and especially establishing possible presence of carbon nanotubes in the samples. The Raman spectrum of carbon (A) is shown in Fig 4a. The spectrum reveals distinctively visible G (ca.  $1580\text{ cm}^{-1}$ ) and G' (ca.  $2670\text{ cm}^{-1}$ ) bands, which

confirm the existence of  $sp^2$  carbon hybrid structure in Carbon A [28]. Simultaneously the presence of a strong D-band at  $1345\text{ cm}^{-1}$  suggests an amorphous carbon phase with embedded crystalline particles. The configuration of D, G, G', and G+D ( $2,916\text{ cm}^{-1}$ ) bands has been found to be characteristic for the existence of carbon nanotubes by other authors [29, 30]. The intensity of the G band (ca.  $1580\text{ cm}^{-1}$ ) is higher than the intensity of the D band (ca.  $1345\text{ cm}^{-1}$ ). There are additional bands detected in the range of  $250\text{--}100\text{ cm}^{-1}$ , corresponding to the radial breathing mode (RBM) bands. All those features are usually observed in the presence of single-walled and double-walled carbon nanotubes (SWCNTs and DWCNTs) [31, 32].



A



B

**Figure 4.** a) The Raman spectra recorded for carbon (A) b). The Raman spectra recorded for carbon (B).

Therefore, we consider a presence of multi-walled carbon nanotubes in the sample (A) plausible. Fig 4b shows the Raman spectrum recorded for carbon black (N-220) The first – order spectrum of the soot generally exhibited two broad and strongly overlapping peaks with maximum at  $\sim 1339\text{ cm}^{-1}$  and at  $\sim 1597\text{ cm}^{-1}$ . A. Sadezky et al [33] suggested, that such Raman spectra of soot can be interpreted in terms of highly disordered graphite structure.

**Table 1.** The elemental composition of carbon (A) and (B) powder surface.

Sample	Atomic concentration (at.%)			
	C 1s	O 1s	S 2p	Cl 2p
Carbon A	98.26	0.97	-	0.07
Carbon B	99.28	0.36	0.35	-

XPS methods were used to obtain additional information about the atomic composition and electronic properties of both carbon powder surfaces [34]. The surface composition of both carbon powders was analysed to the analytic depth of 10.3 nm (see Table 1). It was found that carbon (A) contains more oxygen than carbon (B). The oxygen to carbon ratio was equal to  $9.8 \cdot 10^{-3}$  and  $3.6 \cdot 10^{-3}$  for carbon (A) and (B), respectively. Traces of sulphur were also detected on the surface of carbon (B). The detailed analysis of high resolution C 1s spectrum of both carbons is presented in Fig. 5 and Table 2.

**Table 2.** The parameters of the deconvoluted C 1s and O 1s spectra for both carbons.

Component	Carbon A		Carbon B		Assignment
	BE (eV)	%	BE (eV)	%	
C 1s core excitation					
A	284.4	51.2	284.3	51.1	C-C sp <sup>2</sup>
B	285.3	26.9	285.3	23.4	C-C sp <sup>3</sup>
C	286.4	10.2	286.5	11.1	C-OH + C-O-C
D	288.4	5.6	288.4	6.8	C=O
E	290.9	6.1	290.8	7.6	COOH + CO <sub>3</sub> <sup>2-</sup>
sat	293.4	-	293.4	-	shake-up
O 1s core excitation					
A	531.8	32.2	532.0	42.8	OH, C-O-C, CO <sub>3</sub> <sup>2-</sup>
B	533.3	67.8	533.4	57.2	H <sub>2</sub> O + O <sub>2</sub> <sup>-</sup> in organic compounds
sat	535.9	-	535.8	-	shake-up

The C 1s core excitation shows very similar spectrum envelope for both of the studied samples: carbon (A) and carbon (B). Each spectrum was deconvoluted into five components assigned to specific carbon species and shake-up satellites. The comparison of spectra revealed that carbon (A) and carbon (B) contained similar amount of oxidized species. It was found that each of the oxygen-bonded C 1s spectrum components (C, D and E peaks) exhibited similar increase in signal intensity.

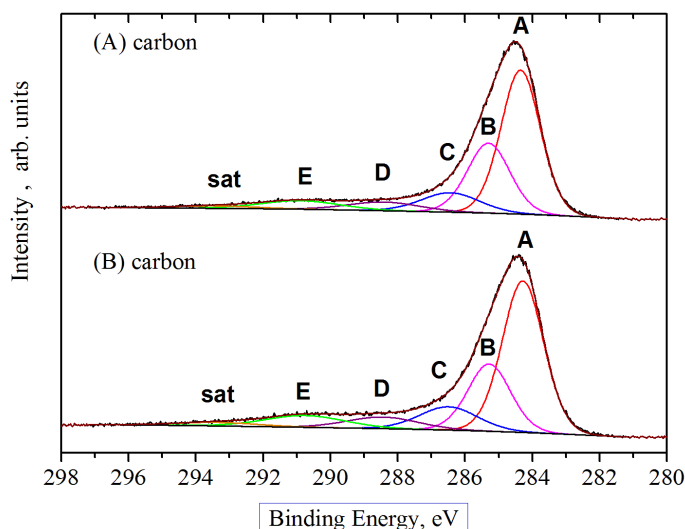


**Figure 5.** The detailed analysis of C1s spectrum

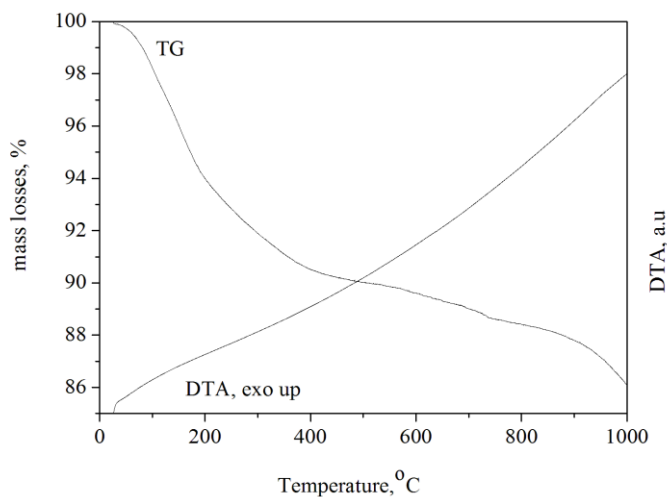
Additionally, the deconvolution of the C 1s spectrum allowed calculation of the ratio of  $sp^2$  to  $sp^3$  forms of carbon. They were equal to 1.90 and 2.18 for carbon (A) and (B), respectively, indicating larger amount of graphite-like carbon in carbon (B) powder. The O 1s spectra were deconvoluted into three components assigned to oxygen in hydroxyl, ether and carbonate groups (A component) or oxygen in water or organic compounds (Table 2). The third component at binding energy (BE) of about 536 eV was assigned to shake-up satellites of  $\pi^*$  electrons. It is worth noticing that O 1s line is a nonspecific excitation where several components can show similar BE at the maximum of the photoelectron spectrum. It was also concluded that the characteristics of the responses attributed to the oxygen components were related to the presence of adsorbed water in the samples (A) and (B), which was more apparent in the former.

The thermal analysis of the samples was performed to investigate the thermal and chemical stability of both carbon fuels in operational conditions of DC-SOFC, i.e. in the temperature range of 600–1000 °C. These data is needed to understand the mechanics and kinetics of the electrochemical carbon oxidation process in the solid oxide fuel cell and to optimize the performance of the DC-SOFC. During the tests of DC-SOFC with 8YSZ electrolyte, helium, argon, CO<sub>2</sub> and gas mixtures of Ar+CO<sub>2</sub> and were tested/experimented as shielding gases.

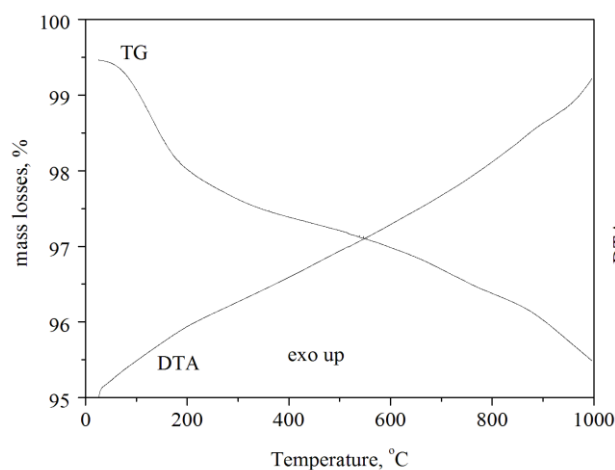
The thermal effects recorded by DTA and TG for powders of both, carbon (A) and (B), heated from 25 to 1000 °C in flowing helium gas atmosphere are presented in Fig. 6a-b. Analysis of TG curves showed two possible regions of carbon mass losses for both carbon powders. Total mass losses of ~10% for Carbon A and ~3% for Carbon B were estimated to take place in the low temperature region (25-500 °C). In the case of sample (A) the higher loss could be attributed to the evaporation of adsorbed water and the decomposition of hydrocarbons group, which were identified by XPS analysis. In the higher temperature region (500-1000 °C), corresponding to the operation temperatures of DC-SOFC, smaller mass losses were observed for both carbon (B) and carbon (A).

Structure and properties of carbon such as crystallinity, surface area, particle size distribution and impurities influence the electrochemical reactivity of carbon [13, 14]. Generally, poorly

crystallized, highly latticed disordered carbons are reported to be more reactive, most probably due to existence of abundant surface defects. Certain advantages of using smaller carbon particles were also observed but the rates of electrochemical oxidation could be correlated to the surface area of carbons. The kinetics of the electrochemical oxidation is affected much stronger by improved wetting effect in the fuel/melt mixtures. Higher wettability results in a better contact of carbon particle with  $O^{2-}$  ions in molten electrolyte [35].



A



B

**Figure 6.** a) DTA, TG curve recorded for carbon powder (A) in helium gas flow atmosphere; b) DTA, TG curve recorded for carbon powder (B) in helium gas flow atmosphere

The problem of choosing an adequate carbon type as a source of fuel to DC-SOFC technology is further complicated by the limited reaction zone in the solid state, restricted to the direct contact between the carbon particles and the surface of solid oxide electrolytes or anode materials. The properties of carbon particles have higher impact on the carbon electrochemical oxidation kinetics in DC-SOFC rather than in the case of liquid electrolytes, where the reaction occurs in the whole fuel

volume. However, despite the growing interest in the DC-SOFC technology, there is still a lack of understanding linking the properties of carbon powders and the performance of DC-SOFC.

Gür [36] reported that graphite oxidizes slowly and reacts with the oxygen only at the edges of the carbon sheets and not on the sheet faces. Thus, increasing the surface to volume ratio of the graphite particles can result in an improved DC-SOFC performance. The micro structural properties of the fuel such as the particle size distribution and the structural disorder also can influence the performance of the DC-SOFCs. Therefore, a systematic investigation of carbon samples properties was performed.

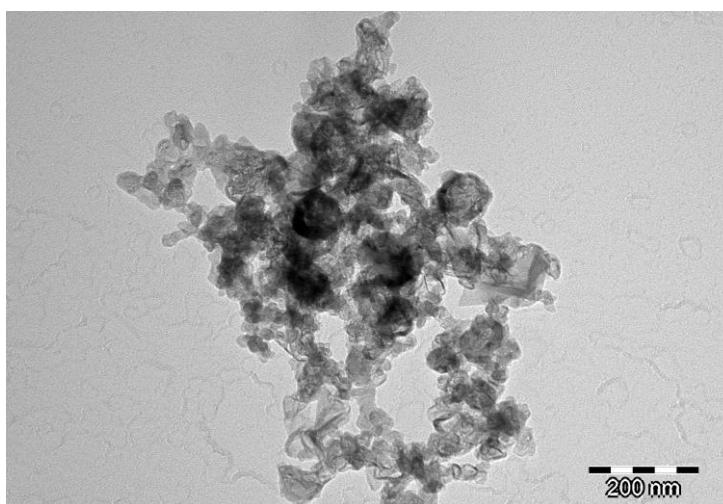
The properties of carbon materials (A) and (B) such as: surface area, crystalline sizes and ash content are summarized in Table 3.

**Table 3.** The properties of carbon samples

Carbon powder	surface area (m <sup>2</sup> /g)	crystalline size d(002)	ash content [%]
carbon A	60.88 ± 0.28	~3.8 nm	< 0.06
carbon B	102.96 ± 1.6	~2.1 nm	< 0.1

The data presented indicate that carbon powder (A) has lower surface area and slightly higher crystalline average particles size  $d_{(002)}$  than carbon black (B). Both samples contain low amount of inorganic compounds (ash) as contamination. Some low content of ash in the fuel utilized in DC-SOFC can be beneficial for reliable long term operation of the cell .

A typical TEM microphotographs of carbon (A) and (B) particles are presented in Fig. 7 a and b. As observed, carbon (A) consists mainly of isometric particles with dimensions ranging from 30 to 60 nm. In the case of the carbon black powder (B), the isometric particles dimensions are ranging from 20 to 40 nm. In both carbon powders investigated, some forms of agglomerates (60-80 nm) were observed.



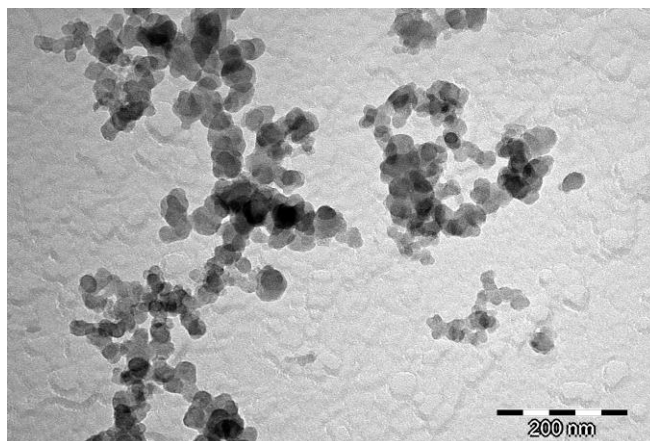


**Figure 7.** A) Typical TEM microphotograph recorded for carbon particles (A); b) Typical TEM microphotograph recorded for carbon particles (B).

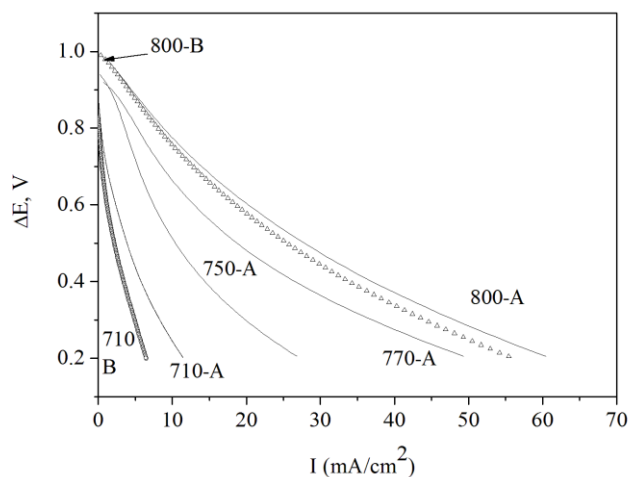
The electrical conductivity of the carbon fuel is an important factor governing the DC-SOFC performance, taking into account that the carbon particles are not only consumed in the electrochemical reaction, but also operate as a current collector. Carbon of high specific electrical resistance increases the total ohmic resistance of the DC-SOFC. This is particularly valid for carbon fuels with higher content of inorganic impurities. On the other hand, some impurities may improve kinetics of electrode reactions due to their catalytic properties.

The estimated values of electrical resistivity of carbon pellets at 25°C were equal to  $\sigma = 0.2$  and  $0.06$  ( $S/cm^2$ ) for the samples (A) and (B) respectively. At 800 °C, the respective values of  $\sigma$  were estimated at  $0.6$  and  $0.36$  ( $S/cm^2$ ). As seen, the carbon (A) powder had systematically lower electrical resistance in the investigated temperature range.

#### Electrochemical investigations

Cell a: C|8YSZ|LSM-GDC|LSM|O<sub>2</sub> (Fig. 1a)

A typical family of curves of the overpotential ( $\Delta E$ ) versus the current density ( $I$ ) (the design of the cell is presented in Fig.1a) at various operating temperatures is shown in Fig. 8a.



A

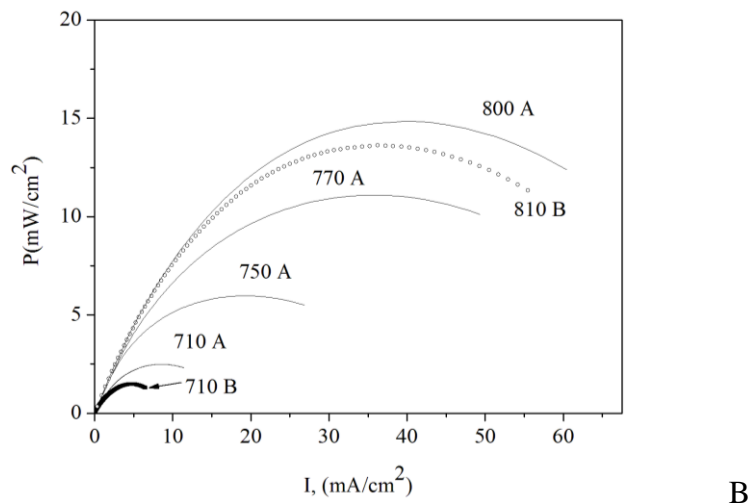


**Figure 8** a) The family of  $\Delta E$ -I dependencies recorded for DC-SOFC with 8YSZ electrolyte of construction shown in Fig.1a; b) The family of P-I dependencies recorded for DC-SOFC with 8YSZ electrolyte (construction of the cell is shown in Fig.1 a)

As can be seen, the voltage ( $\Delta E$ ) of the cell increases with the temperatures. At the temperature of 800 °C, the voltage reached the value ca. 1.02 V, which is close to the reversible voltage of carbon oxidized versus oxygen electrode.

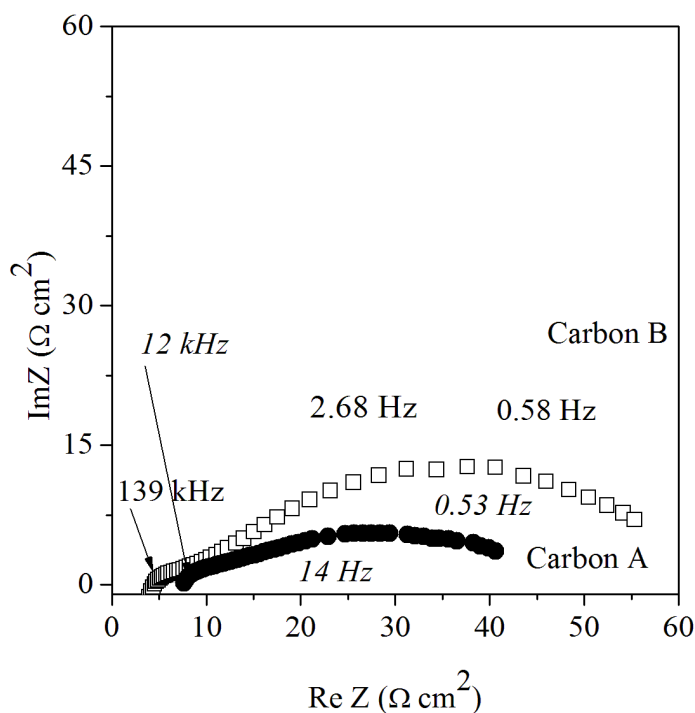


**Figure 9.** The impedance spectra recorded for the DC-SOFC cell fed with carbon (A) and (B) (construction of the cell is shown in Fig. 1a).

Although there is no significant difference between curves shown in Fig. 8a for carbon (A) and (B), the power vs. current curves (presented in Fig. 8b) show that the power densities obtained for the cell supplied with carbon (B) are slightly but systematically lower than those for the cell supplied with carbon (A).

The similar experiments were performed by P. Descalux, et al. [18]. They postulated that the carbon oxidation in the DC-SOFC proceeds almost exclusively according to the reaction:



and the effect of carbon monoxide oxidation can be neglected:



CO is formed in a Boudouard reaction, when the product of the reaction (1), CO<sub>2</sub> reacts with a carbon particle:



At high temperatures, characteristic for the DC-SOFC operations (above 650°C), reaction (3) is shifted to the right side.

The electrochemical oxidation of carbon was also studied by the EIS method. The complex plane plots recorded for the DC-SOFCs fed either with carbon powder (A) or (B) are shown in Fig. 9

Large polarization impedances are observed for both investigated carbons (A) and (B). These can be attributed to the sluggish kinetics of carbon oxidation due to the restricted reaction zone, limited to the direct contacts area between the solid carbon and solid electrolyte. The lower polarization impedance measured for carbon (A) indicates its higher reactivity regarding the electrochemical oxidation in comparison to carbon (B). There are several possible reasons for such behaviour. The lower polarization losses in the case of carbon A could be related e.g. to the highly disordered morphology of carbon A (surface bond termination) or the different degree of carbon particles sintering during the high temperature procedure. The presence of sulphur, which was detected on the surface of carbon powder (B) by the XPS investigations, had also some additional negative effect on the kinetics of electrochemical oxidation of carbon.

Cell b: C+(Li<sub>2</sub>CO<sub>3</sub>-Na<sub>2</sub>CO<sub>3</sub>) eut. |8YSZ|LSM-GDC|LSM|O<sub>2</sub> (Fig. 1b)

One possible way to improve the DC-SOFC performance is to increase the reaction zone of the electrochemical oxidation of the carbon fuel. It can be done by addition of molten carbonate eutectic (Li<sub>2</sub>CO<sub>3</sub>+Na<sub>2</sub>CO<sub>3</sub>) to the carbon fuel as shown in Fig. 1b.

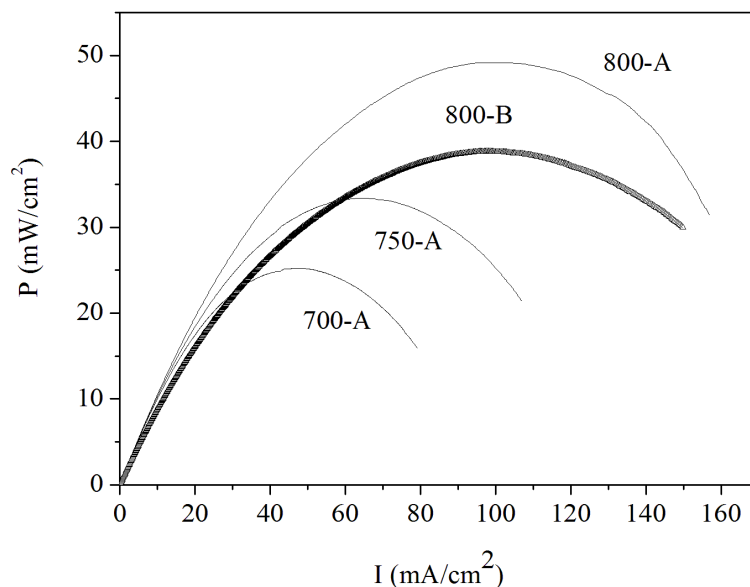


**Figure 10.** Family of  $P$  vs.  $I$  dependences recorded for the DC-SOFC fed with composite fuel consisting of carbon (A) or (B) and carbonate melt (construction of the cell is shown in Fig. 1b).

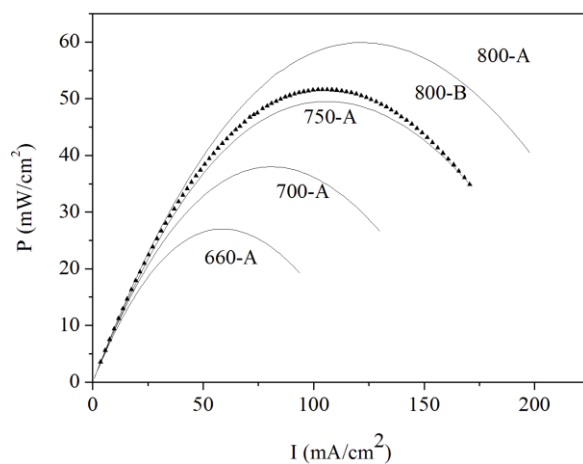
The family of power vs. current density curves recorded for the DC-SOFC supplied with composite fuel consisting of carbon and molten carbonates is presented in Fig. 10. Indeed, the power densities obtained for this type of the cell are about twice as large as those measured for the cell design presented in Fig. 1a. The increase of power and current densities can be explained by the availability of the whole surface of carbon particle to  $O^{2-}$  ions that are present in the melt.

The chemical stability experiments were performed at temperature of 850 °C for 56 h. We examined the cells for evidence of any chemical deterioration by the carbonate melt. The surface of the 8YSZ electrolyte was investigated by XRD and SEM. No products of chemical reaction between the carbonate eutectic ( $Li_2CO_3$ - $Na_2CO_3$ ) or ( $Li_2CO_3$ - $K_2CO_3$ ) and YSZ were revealed by the X-ray diffraction pattern. No cracks or symptoms of chemical corrosion were observed on the surface of solid oxide electrolyte.

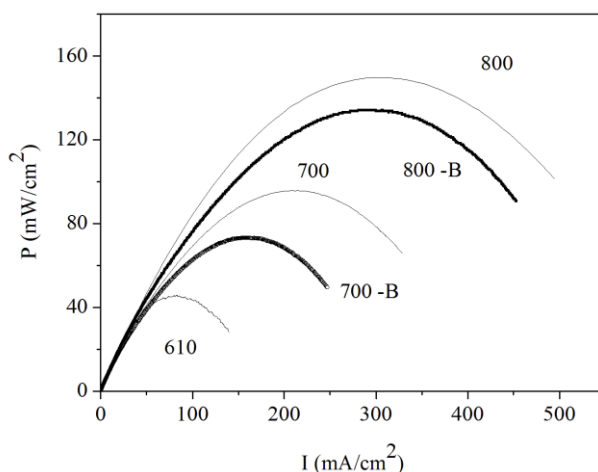
Cell c: C|Ni-YSZ|8YSZ|LSM-GDC|LSM| $O_2$  (Fig. 1c) and

Cell d: C+( $Li_2CO_3$ - $Na_2CO_3$ ) eut. |Ni-YSZ|8YSZ|LSM-GDC|LSM| $O_2$  (Fig. 1d)

When the surface of the solid oxide electrolyte is coated with thin Ni-YSZ anode, the cell is able to utilize not only solid carbon particles but also the gaseous CO produced in the Boudouard reaction (3). Hence, further improvements of performances of these fuel cells were expected. The design of such cells is presented in Figs. 1c and 1d. The cells were supplied, respectively, with pure carbon and carbon+carbonate melt composite fuels. Typical performances of the cells are presented in Fig. 11a and 11b.



A



B

**Figure 11.** a) Family of P vs. I dependences recorded for the DC-SOFC with Ni-YSZ anode fed with carbon (A) or (B) (construction of the cell is shown in Fig. 1c); b) Family of P vs. I dependences recorded for the DC-SOFC with Ni-YSZ anode fed with composite fuel consisting of carbon (A) or (B) and carbonate melt (construction of the cell is shown in Fig. 1d).

As can be seen in Fig. 11a, the power densities of the cell investigated were similar to these obtained for the DC-SOFC of the type presented in Fig. 1b and substantially higher than for the DC-SOFC of the type presented in Fig. 1a. However, it is difficult to conclude if the effect observed can be attributed to either the contribution of reaction (2) or the enlargement of reaction zone by porous structure of anode material.

Recently, Gür [37] proposed “CO shuttle mechanism” to explain the mechanism of carbon oxidation under CO<sub>2</sub> or inert gas atmospheres in several types of direct carbon fuel cells. He suggested that the considered reaction involved oxygen on the carbon surface desorbing as CO into the anode and subsequently undergoing electrochemical oxidation to CO<sub>2</sub> at the TPB. Furthermore, at temperatures above 800 °C, the Boudouard reaction is thermodynamically favorable. In this temperature regime, the surface oxygen desorbs from the carbon particles on the anode surface. CO<sub>2</sub> that formed at the anode

has a short distance to diffuse out to neighbouring carbon particles to the anode surface. The newly formed CO diffuses back to the anode TPB, where is electrochemically oxidized to CO<sub>2</sub>, starting the cycle again.

Significantly better performances were observed for the DC-SOFC with Ni-YSZ anode fed with the composite fuel consisting of carbon and carbonate melts (Fig. 11b). This effect can be explained by the wetting of both carbon particle and electrode material by molten carbonates.

#### 4. CONCLUSION

The experiments described in this work confirm the feasibility of carbon based by-products of natural gas RF plasma reforming as fuel for DC-SOFC. The comparison of the performances of carbon (A) and the commercially available carbon black powder (carbon B) showed consistent albeit slight superiority of the former in the case of four different fuel cell designs. Taking into account that the characterization techniques confirmed that Carbon (B) had larger particles surface area and lower ohmic losses comparing to Carbon (A) we believe that the superior performance of the by-product (Carbon A) is a result of its smaller graphite content and higher surface defects content. Thus the carbon powder, which is a waste product of natural gas plasma splitting, can be considered as viable solid fuel for DCFC technology which along with the efficient hydrogen production by RF plasma natural gas splitting opens alternatives for improving the overall efficiency in the distributed hydrogen and electricity production and storage scenarios.

#### References

1. H.J. Neef, *Energy* 34 2009, 327.
2. S. E. Wright, *Renew Energ.* 29 2004 179
3. N.Z.Muradov, T.N. Veziroğlu, *Int. J Hydrogen Energ* 30 (2005) 225
4. R.M. Navarro, M.A. Pena, J.L.G. Fierro, *Chem. Rev.* 107 (2007) 3952
5. J.T. Overpeck, J.E. Cole, *Annu. Rev. Environ. Resour.* 31 (2006) 1
6. L. Mingyi, YBo, X. Jingming, Ch. Jing, *J Power Sources* 177 (2008) 493
7. Y. Li, D.Li, G. Wang, *Catal. Today* 162 (2011) 1
8. H.F. Abbas, W.M.A. Daud, , *Int. J Hydrogen Energ* 35 (2010) 1160
9. M. Kogan, A. Kogan, *Int. J Hydrogen Energ* 28 (2003) 1187
10. L. Bromberg, L., Cohn, D. R., Rabinovich, A., Alexeev, *Int. J Hydrogen Energ* 24 (1999) 1131
11. Petitpas, G., Rollier, J., Darmon, A., Gonzalezaguilar, J., Metkemeijer, R., Fulcheri, L. *Int. J Hydrogen Energ* 32 (2007) 2848
12. S. Zecevic, E.M. Patton, P. Parhami, *Carbon* 42 (2010) 1893
13. D. CaO, Y.Sun, G. Wang, *J Power Sources* 167 (2007) 250
14. G. Hackett, J. Zondlo, R. Svensson, *J Power Sources* 168 (2007)111
15. X.Li, Z.Zhu, R.Marco, J.Bradley, *J Power Sources* 195 (2010) 4051
16. L.Kouchachvili, M.Ikura, *Int. J Hydrogen Energ* 36 (2011) 10263
17. N.J. Cherepy, NJ Krueger, R.Fiet, K. J Jankowski, *J Electrochem Soc* 2005 (152) A80
18. P. Desclaux, S. Nürnberger, M. Rzepka, U. Stimming, *Int. J Hydrogen Energ* 36 (2011),10278
19. R. Liu, Ch. Zhao, J. Li, F. Zeng, S. Wang, T. Wen, Z.Wen, *J Power Sources* 195 (2010), 480

20. Y. Nabaie, J. T. S. Irvine, *Energy Environ Sci* 1(2008) 148
21. C. Jiang, J.S. Irvine, *J Power Sources* 196 (2011) 7318
22. H. K. Ju, S.Uhm, J. Kim, R. Song, H.Choi, Si.Lee, J.Lee, *J Power Sources* 15 (2012) 36
23. Ch. Li, Y. Shi, N. Cai, 195, *J Power Sources* 15 (2010) 4660
24. M. Dudek, P. Tomczyk, *Catal Today*, 176 (2011) 388
25. E.Z. Kurmaev, S.N. Shamin, K.M. Kolobova, S.V. Shulepov, *Carbon* 24 (1986) 249
26. G. A. Zickler, B.Smarsly, N. Gierlinger, H. Peterlik, O.Paris, *Carbon* 44 (2006) 3229
27. Lu, C. Kong, V. Sahajwalla, D. Harris, *Fuel* 81 (2002) 1215.
28. F. Tuinstra and J. L. Koenig, Raman Spectrum of Graphite, *J Chem Phys* 53 (1970)1126
29. S. Costa, E. Borowiak-Palen, M. Kruszyńska, A. Bachmatiuk, R.J. Kaleńczuk, *Materials Science-Poland*, 26 (2008), 435
30. A. M. Keszler, L. Nemes, S. R. Ahmad, X. Fang, *J Optoelectron Adv M* 6 (2004), 1269
31. J.Chen, X.Yang, Y.Li, *Fuels* 89 (2010) 943
32. T. Shimada, T. Sugai, C. Fantini, M. Souza, L.G. Cançado, A. Jorio, M.A. Pimenta, R. Saito, A. Grüneis, G. Dresselhaus, M.S. Dresselhaus, Y. Ohno, T. Mizutani, H. Shinohara, *Carbon* 43 (2005) 1049
33. A. Sadezky, H. Muckenhuber, H. Grothe, R. Niessner, U. Pöschl, *Carbon* 43 (2005) 1731
34. H.Darmstadt, Ch. Roy, *Carbon* 39 (2001) 841
35. X.Li, Z. Zhu, J.Chen, R.Marco, A. Dicks, J. Bradley, G. Lu, *J Power Sources* 186 (2009) 1
36. T. Gür, *J. Electrochem.Soc.* 139, L95 (1992)
37. T. Gür, *J. Electrochem.Soc.* 175 (5) B571 (2010).